Circle Criterion in Linear Control Design

Marcel Heertjes and Maarten Steinbuch

Abstract— **This paper presents a method for higher-order controller design with improved low-frequent disturbance rejection properties. Given a default PID-based controller, the circle criterion is used to construct an extra controller part that deals with resonances resulting from closing the loop. The advantage is twofold. First, a closed-loop shaping method is obtained that is straightforward, graphically-supported, and intuitively clear. Second, it applies to existing control designs and therefore exploits (or even further extends) the design freedom and low-frequency performances therein. The effectiveness of the method is demonstrated using examples from the wafer scanning industry.**

Index Terms— **absolute stability, circle criterion, frequency-domain methods, loop shaping, PID control, Lyapunov theory**

I. INTRODUCTION

In the field of mechatronics, the application of classical proportional-derivative-integrator (PID) control is widespread. The reason for this seems twofold. On the one hand, its performance under disturbances along with its robustness to model uncertainty sufficiently challenges alternatives. On the other hand, its ease and simplicity of design is difficult to compete with using modern control techniques. On the occasion, however, that higher-order controllers are expected to improve upon the closed-loop performances, standard tuning methodologies and design rules [8] give limited support.

To expand the possibilities of PID-based control, a method is presented using the positive real properties of a default PID design. That is, given the closed-loop frequency response characteristics of such a design and taking into account its positive real properties, an additional closed-loop shaping controller synthesis step is performed using the Nyquist plot. This forms the basis for the derivation of higher-order PID-based filters that allow for a significant controller gain increase and subsequent improvements in low-frequent disturbance suppression; see also [2] with a similar purpose, but under nonlinear feedback conditions.

The paper is organized as follows. In Sec.II, a short introduction into the control of wafer scanners is presented, the latter being a carrier for this work. For motion control systems in general, but wafer scanners in particular, Sec.III provides the conditions for global asymptotic stability of the control design. Based on absolute stability [10], Sec.IV deals with closed-loop shaping in the Nyquist plot, followed, in Sec.V, by relating these stability conditions to classical robustness measures like gain- and phase margin. Improved wafer scanner performance is demonstrated in Sec.VI whereas Sec.VII summarizes the main findings.

II. CONTROL OF WAFER SCANNERS

During the lithographic manufacturing of integrated circuits (ICs) wafer scanners achieve performance by combining nano-scale resolution with optimized wafer throughput; see also [5]. The scanning process can be described as follows, see Fig.1. Light from a laser passes from a reticle
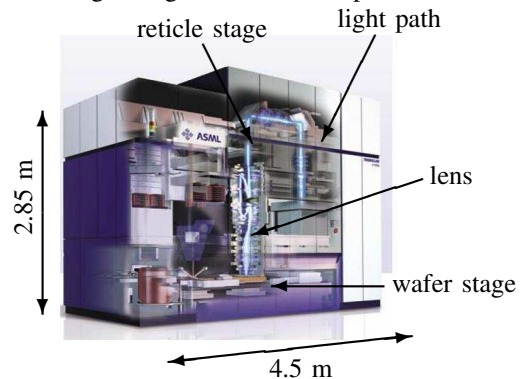

Fig. 1.   Schematic of a wafer scanner.

which contains an image, through a lens, which scales down the image, onto a wafer. Both reticle and wafer are part of two separate motion sub-systems: the reticle stage and the wafer stage. Basically these motion systems represent floating masses which are controlled in six degrees-of-freedom on a single-input single-output (SISO) basis.

For each direction, the reticle- and wafer stage can be represented by the simplified block diagram representation of Fig.2; a more realistic representation using feed forward control and dual-stage feedback falls beyond the scope of this paper. Based on a linear time-invariant PID-based controller
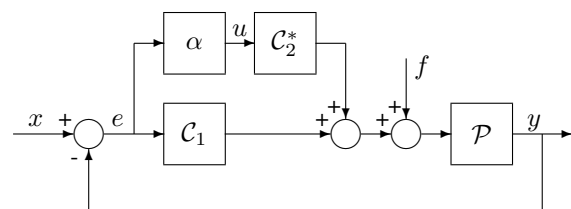

Fig. 2.   Block diagram of the simplified feedback connection.

M.F.Heertjes and M.Steinbuch are with Eindhoven University of Technology, Department of Mechanical Engineering, Eindhoven, The Netherlands m.f.heertjes@tue.nl, m.steinbuch@tue.nl

M.F.Heertjes is also with ASML, Mechatronic Systems Development, Veldhoven, The Netherlands marcel.heertjes@asml.com

C_1, the plant $\mathcal{P}$ is controlled such that its output $y \in \mathbb{R}$ tracks the input $x \in \mathbb{R}$ in face of disturbances (and possible

feed forward contributions) contained in $f \in \mathbb{R}$ or in x itself. The tracking ability is expressed by the servo error signal $e = x - y$. In addition to the lower path from e to y, a path is added given by the series connection of a gain α with $0 \leq \alpha \leq \alpha_{max}$ and a linear time-invariant controller $\mathcal{C}_2^*$ which for reasons of simplicity is chosen $\mathcal{C}_2^* = \mathcal{C}_2\mathcal{C}_1$. The generally higher-order controller $\mathcal{C}_3$ is then given by

$$\mathcal{C}_3 = (1 + \alpha\mathcal{C}_2)\mathcal{C}_1. \tag{1}$$

Both the reticle- and wafer stage plants are characterized by double integrator behavior along with the expression of higher-order dynamics. In this respect, the design of controller $\mathcal{C}_1$ follows a standard loop-shaping argument, see, for example, [8]. A proportional-integrator-derivative (PID) filter is used, which aims at both disturbance rejection and robust stability, a second-order low-pass filter is added to avoid high-frequency noise amplification, and several notch filters are applied to deal with resonant behavior in the plant. For the scanning direction of a wafer stage, the resulting open-loop frequency response functions $\mathcal{O}_l(j\omega) = \mathcal{C}_1(j\omega)\mathcal{P}(j\omega)$ are depicted in Fig.3. In Bode representation, this figure
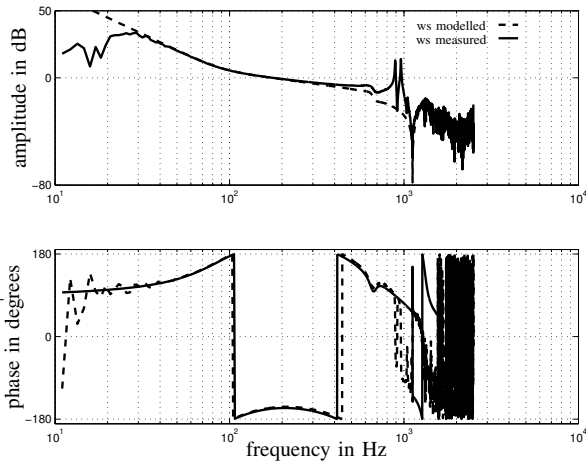

Fig. 3. Bode diagram of the measured open-loop frequency response function of a short-stroke wafer stage in scanning direction along with the characteristics of a second-order plant model.

shows robust stability for both the measured (solid) and modelled (dashed) characteristics.

To design the extra controller $\mathcal{C}_2$ and choose the extra gain α, a loop transformation is performed on the controlled dynamics in Fig.2, the result of which is depicted in Fig.4. Hence a linear time-invariant system in the forward path
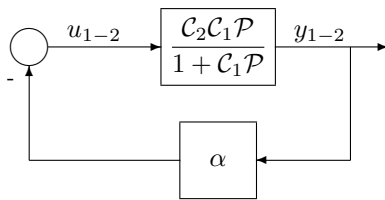

Fig. 4. Block diagram of the transformed feedback connection in Fig.2.

is separated from the gain α in the feedback path with

$u_{1-2} = u_1 - u_2$ and $y_{1-2} = y_1 - y_2$. Note that the pairs $y_1, u_1 \in \mathbb{R}$ and $y_2, u_2 \in \mathbb{R}$ generally differ in terms of initial conditions. If α in Fig.4 is replaced by a memoryless and sector-bounded nonlinearity $0 \leq \alpha(\cdot) \leq \alpha$, this feedback connection shows similarity with a Lurie-Postnikov form [4]. The stability result related to this type of nonlinear systems, which is derived in the next section (Sec.III), is used in the design of $\mathcal{C}_2$ and α via a closed-loop shaping argument. This is considered in Sec.IV.

III. LYAPUNOV STABILITY

Lyapunov stability of systems presented in the feedback connection of Fig.4 (with α being a special case of a generally memoryless and sector-bounded nonlinearity $\alpha(\cdot)$ that satisfies $0 \leq \alpha(\cdot) \leq \alpha$) can be analyzed using the next result.

Theorem 3.1: Assume the strictly proper system $\mathcal{P}$ in Fig.2 that is globally asymptotically stabilized – under uniformly bounded disturbances x and f – by $\mathcal{C}_1$ which is strictly proper and Hurwitz. Also assume $\mathcal{C}_2\mathcal{C}_1$ to be strictly proper and Hurwitz. Then any controller of the form $\mathcal{C}_3 = \mathcal{C}_1 + \alpha\mathcal{C}_2\mathcal{C}_1$ with $0 \leq \alpha \leq \alpha_{max}$ globally asymptotically stabilizes $\mathcal{P}$ in a bounded-input bounded-output sense if

$$\Re\{\mathcal{C}_2(j\omega)\mathcal{G}(j\omega)\} = \Re\left\{\frac{\mathcal{C}_2(j\omega)\mathcal{O}_l(j\omega)}{1 + \mathcal{O}_l(j\omega)}\right\} \geq -\frac{1}{\alpha}. \tag{2}$$

Proof: Since $\mathcal{C}_1$, $\mathcal{C}_2$, and $\mathcal{P}$ are strictly proper functions, $\mathcal{C}_2\mathcal{G}$ is also strictly proper and allows for a state-space realization of the form

$$\begin{aligned}\dot{\mathbf{x}} = & \ \mathbf{A}\mathbf{x} + \mathbf{b}u_{1-2} \\ y_{1-2} = & \ \mathbf{c}^{\mathrm{T}}\mathbf{x},\end{aligned} \tag{3}$$

$\mathbf{x} \in \mathbb{R}^{\mathbf{n}\times\mathbf{1}}$, $\mathbf{A} \in \mathbb{R}^{\mathbf{n}\times\mathbf{n}}$, $\mathbf{b} \in \mathbb{R}^{\mathbf{n}\times\mathbf{1}}$, $\mathbf{c} \in \mathbb{R}^{\mathbf{n}\times\mathbf{1}}$, which in Laplace domain is given by the transfer

$$\frac{y_{1-2}}{u_{1-2}}(s) = \ \mathbf{c}^{\mathrm{T}}(s\mathbf{I} - \mathbf{A})^{-1}\mathbf{b}. \tag{4}$$

Because $\mathcal{C}_1$ globally asymptotically stabilizes $\mathcal{P}$, the closed-loop transfer $\mathcal{P}/(1 + \mathcal{O}_l)$ is Hurwitz, which combined with $\mathcal{C}_2\mathcal{C}_1$ being Hurwitz, gives a $\mathcal{C}_2\mathcal{G}$, hence $\mathbf{A}$, that is Hurwitz. Since the pair $(\mathbf{A}, \mathbf{b})$ is controllable and the pair $(\mathbf{A}, \mathbf{c})$ is observable, a positive definite matrix $\mathbf{P} = \mathbf{P}^{\mathrm{T}} \in \mathbb{R}^{\mathbf{n}\times\mathbf{n}}$, matrix $\mathbf{Q} \in \mathbb{R}^{\mathbf{1}\times\mathbf{n}}$, and a positive constant $\epsilon > 0$ satisfying

$$\begin{aligned}\mathbf{P}\mathbf{A} + \mathbf{A}^{\mathrm{T}}\mathbf{P} = & \ -\mathbf{Q}^{\mathrm{T}}\mathbf{Q} - \epsilon\mathbf{P} \\ \mathbf{P}\mathbf{b} = & \ \mathbf{c} - \sqrt{2}\mathbf{Q}^{\mathrm{T}},\end{aligned} \tag{5}$$

result from $\mathcal{C}_2(j\omega)\mathcal{G}(j\omega)$ satisfying Eq.(2). This is the solution to the Kalman-Yakubovich-Popov problem, see also [1], [6] and the references therein. On the basis of $\mathbf{P}$, the following Lyapunov function candidate is constructed

$$V(\mathbf{x}) = \ \mathbf{x}^{\mathrm{T}}\mathbf{P}\mathbf{x}, \tag{6}$$

which is positive definite and whose derivative is given by

$$\begin{aligned}\dot{V}(\mathbf{x}) = & \ \mathbf{x}^{\mathrm{T}}(\mathbf{A}^{\mathrm{T}}\mathbf{P} + \mathbf{P}\mathbf{A})\mathbf{x} + 2u_{1-2}\mathbf{b}^{\mathrm{T}}\mathbf{P}\mathbf{x} \\ = & \ -\mathbf{x}^{\mathrm{T}}\mathbf{Q}^{\mathrm{T}}\mathbf{Q}\mathbf{x} - \epsilon\mathbf{x}^{\mathrm{T}}\mathbf{P}\mathbf{x} + 2u_{1-2}y_{1-2} \\ & - 2\sqrt{2}u_{1-2}\mathbf{Q}\mathbf{x}.\end{aligned} \tag{7}$$

Since $\alpha u_{1-2} y_{1-2} \leq -u_{1-2}^2$, it follows that

$$
\begin{aligned}
\dot{V}(\mathbf{x}) \leq & -\mathbf{x}^T \mathbf{Q}^T \mathbf{Q} \mathbf{x} - \epsilon \mathbf{x}^T \mathbf{P} \mathbf{x} + 2\mathbf{u_{1-2}^2} \\
& - 2\sqrt{2} u_{1-2} \mathbf{Q} \mathbf{x} \\
\leq & -\epsilon \mathbf{x}^T \mathbf{P} \mathbf{x} - \left(\mathbf{x}^T \mathbf{Q}^T + \sqrt{\mathbf{2}} \mathbf{u_{1-2}} \right)^{\mathbf{2}} \\
\leq & -\epsilon \mathbf{x}^T \mathbf{P} \mathbf{x},
\end{aligned} \tag{8}
$$

which is negative definite, *i.e.*, the equilibrium point $y_{1-2} = y_1 - y_2 = 0$ is globally asymptotically stable whereas the solutions $y_1 = y_1(t)$ and $y_2 = y_2(t)$ are bounded given the imposed stability properties of the control design and the properties of the disturbances x and f. ∎
From Theorem 3.1, it follows that

$$
\left| \frac{\mathcal{C}_2(j\omega)\mathcal{O}_l(j\omega)}{1 + \mathcal{O}_l(j\omega) + \dfrac{\alpha \mathcal{C}_2(j\omega)\mathcal{O}_l(j\omega)}{2}} \right| \leq \frac{2}{\alpha}, \tag{9}
$$

which implies

$$
\Re \left\{ \frac{\dfrac{2}{\alpha} + \dfrac{\mathcal{C}_2(j\omega)\mathcal{O}_l(j\omega)}{1 + \mathcal{O}_l(j\omega) + \dfrac{\alpha \mathcal{C}_2(j\omega)\mathcal{O}_l(j\omega)}{2}}}{-\dfrac{2}{\alpha} + \dfrac{\mathcal{C}_2(j\omega)\mathcal{O}_l(j\omega)}{1 + \mathcal{O}_l(j\omega) + \dfrac{\alpha \mathcal{C}_2(j\omega)\mathcal{O}_l(j\omega)}{2}}} \right\} \leq 0. \tag{10}
$$

As a result, $\mathcal{C}_2 \mathcal{O}_l / (1 + \mathcal{O}_l + \alpha \mathcal{C}_2 \mathcal{O}_l / 2)$ lies in the interior of a circle with radius $2/\alpha$ about the origin. This is the standard circle criterion [3] representation.

For a wafer stage with $\mathcal{C}_2 = 1$, a graphical interpretation of Eq.(9) is shown in Fig.5. Note that global asymptotic stability
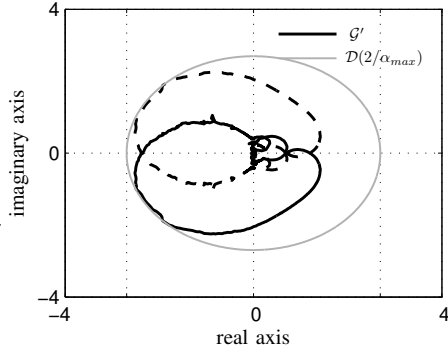

Fig. 5. Nyquist plot of Eq.(9) for a short-stroke wafer stage with $\mathcal{C}_2 = 1$.

is guaranteed if

$$
\mathcal{G}'(j\omega) = \frac{\mathcal{C}_2(j\omega)\mathcal{O}_l(j\omega)}{1 + \mathcal{O}_l(j\omega) + \dfrac{\alpha \mathcal{C}_2(j\omega)\mathcal{O}_l(j\omega)}{2}} \tag{11}
$$

with $0 \leq \alpha \leq \alpha_{max}$ remains in the interior of a disk $\mathcal{D}$ with radius $2/\alpha$ about the origin. Note moreover that for the considered case of $\alpha = \alpha_{max}$, Eq.(2) becomes exact; this fact is used explicitly in the derivation of estimates on robustness margins such as presented in Sec.V. For the special case of $\alpha(\cdot) = \alpha$, stability also follows from the

application of Nyquist's theorem. So what's the contribution of Eq.(2) in view of the results based on linear analysis? Basically, this is the frequency-domain interpretation of Eq.(2), which provides a loop shaping argument (see also [9]) for the design of $\mathcal{C}_2$.

IV. CLOSED-LOOP SHAPING

The design of $\mathcal{C}_2$ in the feedback connection of Figs.2 and 4 is based on closed-loop shaping. Different from the loop-shaping argument used to construct $\mathcal{C}_1$, which deals with resonances in the plant $\mathcal{P}$, the choice for $\mathcal{C}_2$ addresses resonance resulting from closing the loop. A proper choice for $\mathcal{C}_2$ therefore aims at reducing the negative real parts of $\mathcal{G}$ which otherwise endangers the stability result. At the same time, the low-frequency response vectors (with positive real part) should not be decreased too much in magnitude. This assures a potential gain increase not to be counteracted by a decrease in magnitude of these vectors.

Conjecture 4.1: Assume the strictly proper system $\mathcal{P}$ that is globally asymptotically stabilized under the conditions considered in Theorem 3.1. Suppose there exists a filter $\mathcal{C}_2 = \mathcal{C}_2^i$,

$$
\mathcal{C}_2^i(j\omega) = \begin{cases} 1, & \text{if } \Re\{\mathcal{G}(j\omega)\} \geq -1/\alpha, \\ -\dfrac{1}{\alpha \Re\{\mathcal{G}(j\omega)\}}, & \text{if } \Re\{\mathcal{G}(j\omega)\} < -1/\alpha, \end{cases} \tag{12}
$$

which satisfies these conditions. Then the maximum gain value $\alpha = \alpha_{max} > 0$ can be chosen arbitrarily large.

Proof: With $\mathcal{C}_2 = \mathcal{C}_2^i$, Eq.(2) can be written as $\mathcal{C}_2^i(j\omega)\Re\{\mathcal{G}(j\omega)\} \geq -1/\alpha$ which is satisfied for any $\alpha > 0$. ∎

Unfortunately $\mathcal{C}_2^i$ is unstable which for $\Re\{\mathcal{G}(j\omega)\} < -1/\alpha$ follows from

$$
\begin{aligned}
\mathcal{C}_2^i(j\omega) &= -\frac{1}{\alpha} \Re \left\{ \frac{1}{\mathcal{G}(j\omega)} \right\} \\
&= -\frac{1}{2\alpha} \left\{ \frac{1}{\mathcal{G}(j\omega)} + \frac{1}{\mathcal{G}^c(j\omega)} \right\},
\end{aligned} \tag{13}
$$

i.e., $\mathcal{G}(j\omega)$ has left half-plane zeros such that $\mathcal{G}^c(j\omega)$ has right half-plane zeros giving right half-plane poles for $\mathcal{C}_2^i$ if $\Re\{\mathcal{G}(j\omega)\} < -1/\alpha$. But the value of $\mathcal{C}_2^i$ lies in its frequency-domain characteristics which form a reference towards shaping stable filters. This is shown in Fig.6 where it can be seen that a stable wafer stage feedback is obtained for $0 \leq \alpha \leq \alpha_{max} = 5.1282$. For $\mathcal{C}_2 = 1$, this reduces to $\alpha_{max} = 0.7418$. So closed-loop shaping gives a potential gain ratio increase of $(1+5.1282)/(1+0.7418) = 3.5$.

In Bode representation, Fig.7 depicts the magnitude of $\mathcal{C}_2^i$. Note the strong correlation between $\mathcal{C}_2^i$ and two physical realizations $\mathcal{C}_2^1$ and $\mathcal{C}_2^2$. This demonstrates the value of $\mathcal{C}_2^i$ in being a design reference. Having $\mathcal{C}_2$ and α_{max}, the choice of extra gain α amounts to requiring sufficient robustness properties of the control design.

V. ROBUSTNESS MEASURES

The choice of extra gain α largely depends on the choice for the controller $\mathcal{C}_2$, the properties of the closed-loop
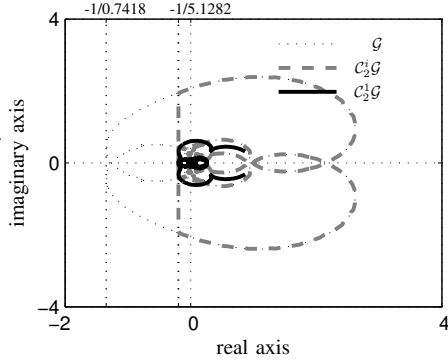
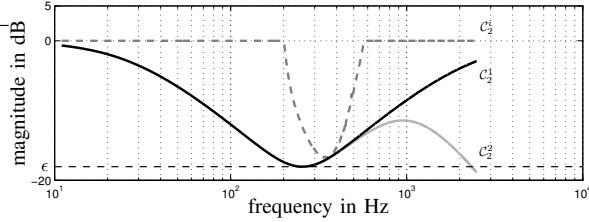Fig. 6. Nyquist plot of Eq.(2) for $\mathcal{G}$, $\mathcal{C}_2^i\mathcal{G}$, and $\mathcal{C}_2^1\mathcal{G}$.

Fig. 7. Bode magnitude plot of $\mathcal{C}_2^i$ and two physical realizations of $\mathcal{C}_2$.

frequency response $\mathcal{G}$ and the requirements imposed on robustness to model error. Herein the relation with classical robustness measures like gain- and phase margin is fundamental. In studying this relation, the positive real properties of $\mathcal{C}_2\mathcal{G}$ are related to bounds on closed-loop sensitivities.

Definition 5.1: For $0 \leq \alpha \leq 2\alpha_{max}$ let $\mathcal{S}(\alpha)$ be the closed-loop sensitivity function:

$$\mathcal{S}(\alpha) = \frac{1}{1 + \mathcal{O}_l + \dfrac{\alpha\mathcal{C}_2\mathcal{O}_l}{2}}, \tag{14}$$

and let $\mathcal{S}_c(\alpha)$ be the complementary sensitivity function:

$$\mathcal{S}_c(\alpha) = \frac{\mathcal{O}_l + \dfrac{\alpha\mathcal{C}_2\mathcal{O}_l}{2}}{1 + \mathcal{O}_l + \dfrac{\alpha\mathcal{C}_2\mathcal{O}_l}{2}}. \tag{15}$$

Corollary 5.1: Assume the strictly proper system $\mathcal{P}$ that is globally asymptotically stabilized under the conditions considered in Theorem 3.1. Moreover, assume that $\epsilon \leq |\mathcal{C}_2(j\omega)|$ with $\epsilon > 0$. Then the closed-loop system satisfies

$$|\mathcal{S}_c(\alpha)| \leq 1 + \frac{2}{\alpha\epsilon}. \tag{16}$$

in terms of complementary sensitivity and

$$|\mathcal{S}(\alpha)| \leq 2 + \frac{2}{\alpha\epsilon}, \tag{17}$$

in terms of sensitivity.

Proof: With Eq.(9), it both follows that

$$\left| \frac{\dfrac{\alpha\mathcal{C}_2(j\omega)\mathcal{O}_l(j\omega)}{2}}{1 + \mathcal{O}_l(j\omega) + \dfrac{\alpha\mathcal{C}_2(j\omega)\mathcal{O}_l(j\omega)}{2}} \right| \leq 1, \tag{18}$$

and

$$\left| \frac{\mathcal{O}_l(j\omega)}{1 + \mathcal{O}_l(j\omega) + \dfrac{\alpha\mathcal{C}_2(j\omega)\mathcal{O}_l(j\omega)}{2}} \right| \leq \frac{2}{\alpha}\frac{1}{|\mathcal{C}_2(j\omega)|} \leq \frac{2}{\alpha\epsilon}, \tag{19}$$

which combined gives Eq.(16). Moreover, using the fact that $||\mathcal{S}| - |\mathcal{S}_c|| \leq |\mathcal{S} + \mathcal{S}_c| = 1$ gives Eq.(17). ∎

Note that the lower bound ϵ on $\mathcal{C}_2$ can be relaxed for all ω sufficiently outside the regions where $\mathcal{S}$ and $\mathcal{S}_c$ have their maximums, thus enabling low-pass characteristics, see Fig.7. For a wafer stage, a graphical representation of Corollary 5.1 is shown in Fig.8. It shows two cases: i) $\mathcal{C}_2 = 1$ with $\alpha = \alpha_{max}/2 \approx 0.7418/2$, and ii) $\mathcal{C}_2 = \mathcal{C}_2^2$ (see Fig.6) with $\alpha = \alpha_{max}/2 \approx 5.1282/2$. Conservatism is included in two ways:
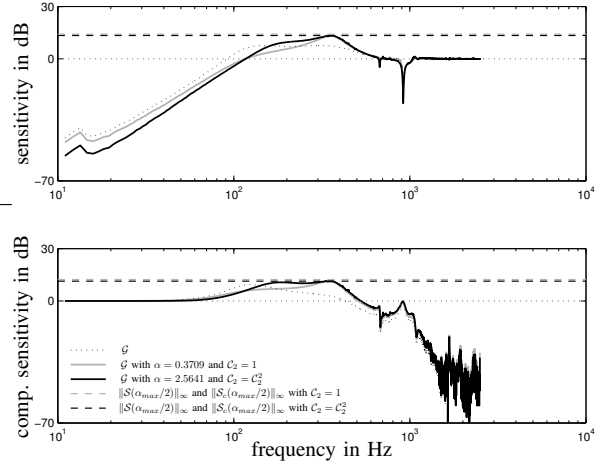

Fig. 8. Bode magnitude plots of frequency response functions and bounds on $\mathcal{S}(\alpha_{max})$ and $\mathcal{S}_c(\alpha_{max})$, respectively.

i) via the lower bound ϵ on $\mathcal{C}_2$, and ii) by obtaining an upper bound on $\mathcal{S}$ using $||\mathcal{S}| - |\mathcal{S}_c|| \leq 1$. As a result only the bound on $\mathcal{S}_c$ for $\mathcal{C}_2 = 1$ with $\alpha = \alpha_{max}$ is exact. Note the potential improvement in low-frequency performance (black curves) in comparison with the reference design (dotted curves) and the reference design with increased gain (grey curves).

Via circle constraints (m-circles [7]), Corollary 5.1 can be used to derive lower bounds on classical robustness measures like gain- and phase margin. Hereto Eq.(16) is written as

$$\left| 1 + \frac{1}{\mathcal{O}_l(j\omega) + \dfrac{\alpha\mathcal{C}_2(j\omega)\mathcal{O}_l(j\omega)}{2}} \right| \geq \frac{\alpha\epsilon}{2 + \alpha\epsilon} = \mathcal{B}_c(\alpha), \tag{20}$$

for all $0 \leq \alpha \leq \alpha_{max}$. In terms of margins, it follows that:

$$\text{gain margin} \geq \frac{1}{1 + \mathcal{B}_c(\alpha)}, \tag{21}$$

$$\text{phase margin} \geq 2\arcsin\left\{ \frac{\mathcal{B}_c(\alpha)}{2} \right\}. \tag{22}$$

This is shown in Fig.9. In Nyquist representation the inverse open-loop frequency responses are shown for: i) $\mathcal{C}_2 = 1$ and

$\alpha = \alpha_{max} \approx 0.7418$, and ii) $\mathcal{C}_2 = \mathcal{C}_2^2$ from Fig.7 with $\epsilon = 1/8$ and $\alpha = \alpha_{max} \approx 5.1282$. With Eq.(21), the gain margins

Fig. 9. Nyquist plot of wafer stage inverse open-loop characteristics and M-circles.
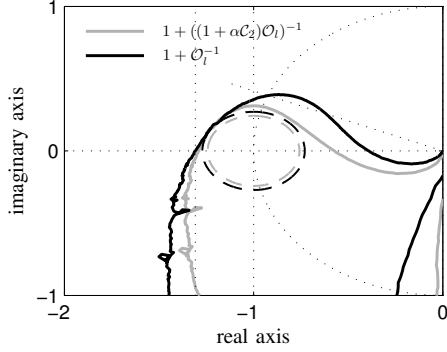

Fig. 10. Nyquist plot of wafer stage open-loop characteristics and M-circles.

of -2.1 dB and -1.9 dB are lower bounds on the actual gain margins of -2.3 dB and -2.2 dB, respectively. In terms of phase margin, Eq.(22) gives 15.6 degrees and 13.9 degrees, respectively, instead of the actual values of 22.3 degrees and 17.9 degrees, respectively. It is therefore concluded that in addition to the previous arguments, the lower bounds in Eqs.(21) and (22) incorporate extra conservatism.

Lower bounds can also be derived on the basis of Eq.(17), however, inducing more conservatism. Namely with

$$\left| 1 + \mathcal{O}_l(j\omega) + \frac{\alpha \mathcal{C}_2(j\omega)\mathcal{O}_l(j\omega)}{2} \right| \geq \frac{\alpha\epsilon}{2 + 2\alpha\epsilon} = \mathcal{B}_s(\alpha), \tag{23}$$

where $0 \leq \mathcal{B}_s(\alpha) \leq \mathcal{B}_c(\alpha)$, it follows that

$$\text{gain margin} \geq 1 - \mathcal{B}_s(\alpha) = 1/(1 + \mathcal{B}_c(\alpha)), \tag{24}$$

which equals the result in Eq.(21). But the lower bound on the phase margin,

$$\begin{aligned} \text{phase margin} &\geq 2\arcsin\left\{ \frac{\mathcal{B}_c(\alpha)}{2} \right\} \\ &\geq 2\arcsin\left\{ \frac{\mathcal{B}_s(\alpha)}{2} \right\}, \end{aligned} \tag{25}$$

becomes more conservative.

A graphical validation of the lower bounds based on Eq.(17) is given in Fig.10. It shows the open-loop frequency responses in Nyquist representation for: i) $\mathcal{C}_2 = 1$ and $\alpha = \alpha_{max} \approx 0.7418$, and ii) $\mathcal{C}_2 = \mathcal{C}_2^2$ with $\epsilon = 1/8$ and $\alpha = \alpha_{max} \approx 5.1282$. In terms of phase margins, the lower bounds are given by 12.2 degrees and 11.2 degrees, respectively. This is an extra decrease as compared to the values obtained from Fig.9, which equal 15.6 degrees and 13.9 degrees, respectively.

Corollary 5.2: Assume the strictly proper system $\mathcal{P}$ that is globally asymptotically stabilized under the conditions considered in Theorem 3.1. Moreover, assume that $\epsilon \leq |\mathcal{C}_2(j\omega)|$ with $\epsilon > 0$. Then the gain- and phase margins satisfy
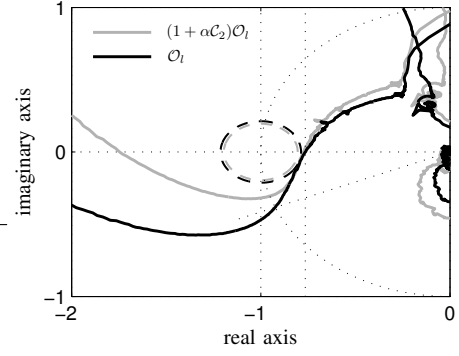
$$\begin{aligned} &\text{for } 0 \leq \alpha \leq \frac{\alpha_{max}}{2} \\ &\qquad \text{gain margin} \geq 1 - \mathcal{B}_{s,1}(\alpha), \\ &\qquad \text{phase margin} \geq 2\arcsin\left\{ \frac{\mathcal{B}_{s,1}(\alpha)}{2} \right\}, \\ &\text{and for } \frac{\alpha_{max}}{2} \leq \alpha \leq \alpha_{max} \\ &\qquad \text{gain margin} \geq 1 - \mathcal{B}_{s,2}(\alpha), \\ &\qquad \text{phase margin} \geq 2\arcsin\left\{ \frac{\mathcal{B}_{s,2}(\alpha)}{2} \right\}, \end{aligned} \tag{26}$$

with

$$\begin{aligned} \mathcal{B}_{s,1}(\alpha) &= \frac{1}{\|\mathcal{S}(0)\|_\infty} - \frac{2\alpha \mathcal{B}_s(\alpha_{max}/2)}{\alpha_{max}}, \\ \mathcal{B}_{s,2}(\alpha) &= 2\mathcal{B}_s(\alpha_{max}/2) - \frac{2\alpha \mathcal{B}_s(\alpha_{max}/2)}{\alpha_{max}}. \end{aligned} \tag{27}$$

Proof: From Eqs.(9) and (23) at $\alpha = \alpha_{max}$, it follows that

$$\begin{aligned} -|\alpha \mathcal{C}_2 \mathcal{O}_l| &\geq -\frac{2\alpha}{\alpha_{max}} \left| 1 + \mathcal{O}_l + \frac{\alpha_{max}\mathcal{C}_2\mathcal{O}_l}{2} \right| \\ &\geq -\frac{2\alpha \mathcal{B}_s(\alpha_{max}/2)}{\alpha_{max}}, \ 0 \leq \alpha \leq \frac{\alpha_{max}}{2}, \end{aligned} \tag{28}$$

hence

$$\begin{aligned} |1 + \mathcal{O}_l + \alpha \mathcal{C}_2\mathcal{O}_l| &\geq |1 + \mathcal{O}_l| - |\alpha \mathcal{C}_2\mathcal{O}_l| \\ &\geq |1 + \mathcal{O}_l| - \frac{2\alpha \mathcal{B}_s(\alpha_{max}/2)}{\alpha_{max}} \\ &\geq \frac{1}{\|\mathcal{S}(0)\|_\infty} - \frac{2\alpha \mathcal{B}_s(\alpha_{max}/2)}{\alpha_{max}}, \end{aligned} \tag{29}$$

which combined with Eqs.(24) and (25) gives the first part in Eq.(26). For the second part, Eq.(9) at $\alpha = \alpha_{max}$ is written as

$$\begin{aligned} -\left| \left(\alpha - \frac{\alpha_{max}}{2}\right)\mathcal{C}_2\mathcal{O}_l \right| &\geq \left| 1 + \mathcal{O}_l + \frac{\alpha_{max}\mathcal{C}_2\mathcal{O}_l}{2} \right| \left(1 - \frac{2\alpha}{\alpha_{max}} \right) \\ &\geq \mathcal{B}_s(\alpha_{max}/2)\left(1 - \frac{2\alpha}{\alpha_{max}} \right), \end{aligned} \tag{30}$$

for $\frac{\alpha_{max}}{2} \leq \alpha \leq \alpha_{max}$, which gives

$$
\begin{aligned}
&|1 + \mathcal{O}_l + \alpha \mathcal{C}_2 \mathcal{O}_l| = \\
&\left|1 + \mathcal{O}_l + \frac{\alpha_{max}\mathcal{C}_2\mathcal{O}_l}{2} + \left(\alpha - \frac{\alpha_{max}}{2}\right)\mathcal{C}_2\mathcal{O}_l\right| \\
&\geq \left|1 + \mathcal{O}_l + \frac{\alpha_{max}\mathcal{C}_2\mathcal{O}_l}{2}\right| - \left|\left(\alpha - \frac{\alpha_{max}}{2}\right)\mathcal{C}_2\mathcal{O}_l\right| \\
&\geq 2\mathcal{B}_s(\alpha_{max}/2) - \frac{2\alpha\mathcal{B}_s(\alpha_{max}/2)}{\alpha_{max}},
\end{aligned}
\tag{31}
$$

and combined with Eqs.(24) and (25) completes the proof. ∎

If $1/\|\mathcal{S}(0)\|_\infty = 2\mathcal{B}_s(\alpha_{max}/2)$, Corollary 5.2 states that the m-circles evolution along α can be approximated by a linear descent from the original values at $\alpha = 0$ to zero (for the phase margin) and one (for the gain margin) at $\alpha = \alpha_{max}$. In an approximative sense, the same reasoning can be applied on the actual stability margins, see Fig.11, which gives direction during the process of tuning α.

A graphical validation of the lower bounds in Eq.(26) is given in Fig.11. It shows that these bounds provide fairly
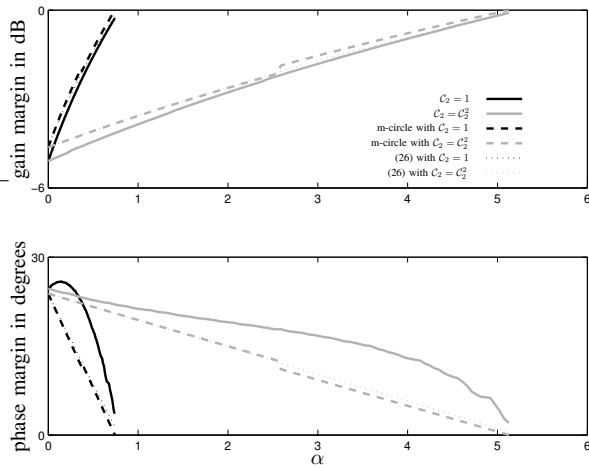

Fig. 11. Gain- and phase margins (solid curves) compared with m-circle estimates (dotted curves) and lower bounds (dashed curves) based on Eq.(26) for a design with $\mathcal{C}_2 = 1$ (black curves) and a design with $\mathcal{C}_2 = \mathcal{C}_2^2$ (grey curves).

good estimates on the bounds obtained by computing the m-circles, the latter providing reasonable estimates for the actual gain margins. The estimates for the actual phase margins, however, possess significant conservatism, the source of which is previously discussed.

VI. WAFER STAGE PERFORMANCE

Improved wafer stage performance is demonstrated in Fig.12. Both in time-domain or via cumulative power spectral density analysis (cpsd), the effect on the error e is demonstrated of an open-loop shaped (default) controller $\mathcal{C}_1$ (grey curves) and a combined open-loop/closed-loop shaped controller $\mathcal{C}_3$ (black curves with $\alpha = 3$). The wafer stage is subjected to an acceleration set-point profile (dotted curve) which is repeated four times. Characteristic to the combined
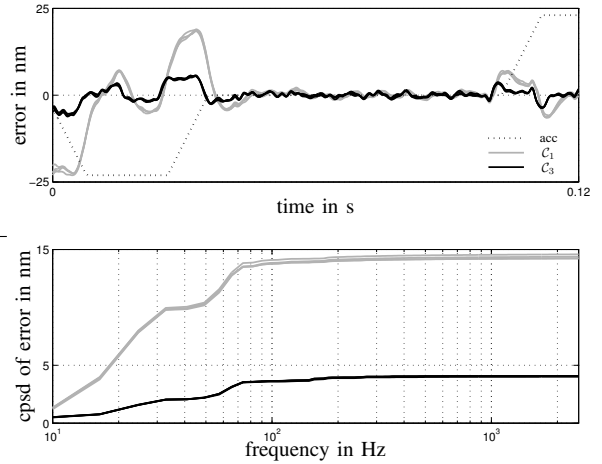

Fig. 12. Time-series measurement and cumulative power spectral densities of a design based on $\mathcal{C}_1$ (grey) and $\mathcal{C}_3$ (black) with $\alpha = 3$.

loop shaping strategy and design of $\mathcal{C}_3$, a significant low-frequent improvement results. Note that the ultimate (low-frequent) improvement by a factor of $1+\alpha$ is largely realized.

VII. CONCLUSIONS

For motion systems, a method to obtain higher-order controllers embedded in a default PID-based design is presented. Herein the properties of the default design generally allow for a closed-loop shaping argument derived from the circle criterion. In view of lower bounds on classical robustness measures such as gain- and phase margin, this gives the possibility of improved low-frequency performance, the latter being the result of a substantial gain increase. The effectiveness of the approach is demonstrated on the wafer stage of an industrial wafer scanner.

REFERENCES

[1] Haddad WM, and Bernstein DS. (1991) Explicit Construction of Quadratic Lyapunov Functions for the Small Gain, Positivity, Circle, and Popov Theorems and Their Application to Robust Stability. In Proceedings of the Conference on Decision and Control, Brighton, England: 2618-2623.
[2] Heertjes MF, Cremers FLM, Rieck M, and Steinbuch M. (2005) Nonlinear control of optical storage drives with improved shock performance. Control Engineering Practice, 13:1295-1305.
[3] Khalil HK. (1996) Nonlinear Systems - second edition. Prentice Hall, New York.
[4] Lurie AI, and Postnikov VN. (1944) On the theory of stability of control systems. Journal of Applied Mathematics and Mechanics, 8(3):246-248.
[5] Mishra S, Coaplen J, and Tomizuka M. (2007) Segmented iterative learning control for nonrepetitive disturbances. IEEE Control Systems Magazine, August:20-25.
[6] Rantzer A. (1996) On the Kalman-Yakubovich-Popov lemma. Systems & Control Letters, 28:7-10.
[7] Skogestad S, and Postlethwaite I. (2005) Multivariable Feedback Control - Analysis and Design. John Wiley & Sons, England.
[8] Steinbuch M and Norg ML. (1998) Advanced motion control: an industrial perspective. European Journal of Control, 4: 278-293.
[9] Xia L, and Messner W. (2007) Loop shaping with the circle criterion-Bode plot with application to active tape steering. In Proceedings of the American Control Conference, New York, USA: 37-42.
[10] Yakubovich VA. (1964) The matrix inequality method in the theory of the stability of nonlinear control systems - i. the absolute stability of forced vibrations. Automation and Remote Control, 7:905-917.